Inorganic Chemistry

Article

pubs.acs.org/IC

Reactions of Lanthanide Atoms with Oxygen Difluoride and the Role of the Ln Oxidation State

Tanya Mikulas,[†] Mingyang Chen,[†] David A. Dixon,*[,†] Kirk A. Peterson,[‡] Yu Gong,[§] and Lester Andrews*[,§]

[†]Department of Chemistry, The University of Alabama, Shelby Hall, Tuscaloosa, Alabama 35487-0336, United States

[‡]Department of Chemistry, Washington State University, Pullman, Washington 99164-4630, United States

[§]Department of Chemistry, University of Virginia, Charlottesville, Virginia 22904-4319, United States

Supporting Information

ABSTRACT: Laser-ablated lanthanide metal atoms were condensed with OF_2 in excess argon or neon at 4 K. New infrared absorption bands were observed and assigned to the oxidative addition products $OLnF_2$ and OLnF on the basis of ^{18}O isotopic substitution and electronic structure calculations of the vibrational frequencies. The dominant absorptions in the 500 cm^{-1} region are identified as Ln−F stretching modes, which follow the lanthanide contraction. The Ln−O stretching frequency is an important measure of the oxidation states of the Ln and oxygen and the spin state of the complex. The $OCeF_2$, $OPrF_2$, and $OTbF_2$ molecules have higher frequency Ln−O stretching modes. The Ce is assigned to the IV oxidation state and the Pr and Tb are assigned to a mixed III/IV oxidation state. The remaining $OLnF_2$ compounds have lower Ln−O stretches, and the Ln is in the III oxidation state and the O is in the −1 oxidation state. For all of the OLnF compounds, the metal is in the III oxidation state, and the Ln−F bonds are ionic. In $OCeF_2$, OLaF, and OLuF, the bonding between the Ln and O is best described as a highly polarized σ bond and two pseudo π bonds formed by donation from the two 2p lone pairs on the O to the Ln. Bonding for the $OLnF_2$ compounds in the III oxidation state is predicted to be fully ionic. The bonding in $OLnF_2$ and OLnF is dominated by the oxidation state on the lanthanide and the spin state of the molecule. The observation of larger neon to argon matrix shifts for Ln−O modes in several OLnF molecules as compared to their $OLnF_2$ analogues is indicative of more ionic character in the OLnF species, consistent with the more formal negative charge on the oxygen in OLnF.

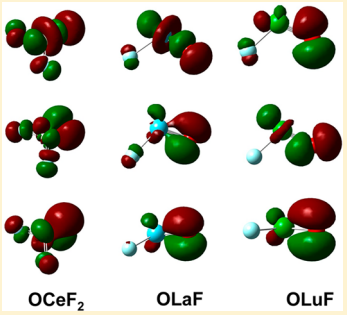

INTRODUCTION

There is substantial interest in the properties of lanthanides and actinides, particularly the role of the valence d and f orbitals in the bonding of ligands to the metal center.[1] The reactions involving lanthanide atoms exhibit trends across the series because of the presence of electrons in the 4f orbitals, even though the 4f electrons are often not very involved in the bonding in molecules containing the lanthanides. The reaction mechanisms and the product structures are determined by the electronic properties of the free lanthanide atoms and the oxidation state/electronic structure in the reaction products. We have been particularly interested in the reactions of lanthanide atoms with simple molecules including CH_3F,[2] CH_2F_2,[3] CHF_3,[4] and CH_3OH,[5] and especially in the bonding between the Ln and CRR′ groups. These reactions have been studied by infrared spectroscopy in cryogenic matrixes coupled with electronic structure investigations of the products. Additional studies of the reactions of other small molecules with lanthanide metals, particularly O_2, H_2, H_2O, N_2, and NO, with the products isolated in matrixes have been reported.[6−21]

Oxygen difluoride is a useful reagent for reacting with laser ablated metals. The reaction of OF_2 with early actinides Th and U yielded the oxide fluorides $OThF_2$ and OUF_2, and reaction with the Group 3 and Group 4 transition metals yielded both oxide fluorides OMF and OMF_2.[22,23] The product molecules provide insight into metal oxygen multiple bonding. For example, the early actinide species exhibit polarized triple bonds based on a CASPT2 analysis of the bonding.[24] We now provide the results for the reactions of OF_2 with the lanthanides.

EXPERIMENTAL AND COMPUTATIONAL METHODS

The experimental apparatus and procedure for preparation and characterization of metal atom reaction product molecules in excess argon at 4 K have been described previously.[6,7,25−27] The Nd:YAG laser fundamental (1064 nm, 10 Hz repetition rate with 10 ns pulse width) was focused (10−20 mJ/pulse at the sample) onto a freshly cleaned lanthanide metal target (Johnson-Matthey) mounted on a rotating rod. Laser-ablated lanthanide atoms were codeposited with 3−4 mmol of argon (Matheson, research) containing 1.0% OF_2 (Ozark-Mahoning) onto a CsI cryogenic window for 60 min. The $^{18}OF_2$ sample (91% ^{18}O enriched) was synthesized and kindly provided by Arkell and co-workers.[28] Both OF_2 and $^{18}OF_2$ samples were used without further purification in a passivated stainless steel vacuum

Received: September 24, 2013
Published: December 17, 2013

   dx.doi.org/10.1021/ic402422h | Inorg. Chem. 2014, 53, 446−456

manifold. FTIR spectra were recorded at 0.5 cm^{-1} resolution on a Nicolet 750 FTIR instrument with a HgCdTe range B detector. Matrix samples were annealed at different temperatures and cooled back to 4 K for spectral acquisition. Selected samples were subjected to broadband photolysis by a medium-pressure mercury arc street lamp (Philips, 175W) with the outer globe removed.

Electronic structure calculations, including geometry optimizations and predictions of vibrational frequencies, were done at the density functional theory (DFT) level using the B3LYP hybrid functional[29,30] with the DZVP2 basis set[31] for F and O and the Stuttgart small core relativistic effective core potential (ECP) with its accompanying segmented basis set for the lanthanides[32,33] using Gaussian 09.[34] The enthalpies at 0 K for reactions 1 and 2

$$Ln + OF_2 \rightarrow OLnF_2 \quad (1)$$

$$Ln + OF_2 \rightarrow OLnF + F \quad (2)$$

for the ground and excited spin states of OLnF were calculated. For $OTbF_2$, the BP86 exchange-correlation functional[35,36] was used because of excessive symmetry breaking with the B3LYP functional. For the three OLnF molecules with Ln = Eu, Gd, and Yb, it was not possible to obtain good agreement with the experimental frequencies with either functional because of spin contamination. For these three OLnF molecules, we used the method of coupled-cluster with single and double and perturbative triple excitations CCSD(T)[37−39] with the aug-cc-pVDZ basis set[40] on O and F and the same ECP and segmented basis described above (ECP28MWB) for the lanthanides. The CCSD(T) calculations were done within the frozen core approximation (2s2p electrons correlated for O, F and 5s5p5d4f for the lanthanide atoms) with the MOLPRO 2010.1 program system[41] with open shell molecules treated at the R/UCCSD(T) level (a restricted open shell Hartree−Fock (ROHF) calculation for the starting wave function with the spin constraint relaxed in the coupled cluster calculation).[42−44]

RESULTS AND DISCUSSION

Metal independent IR absorptions were observed in all of the lanthanide and OF_2 reactions. The absorption at 1028.1 cm^{-1} is the vibrational fundamental of the OF radical,[45,46] and the OF absorbance on sample deposition increased with increasing laser energies. This band decreased during sample annealing, but increased when broad band irradiation (λ > 220 nm) was used (Figure 1). In addition, several other weak absorptions due to CF_4, CO, CO_2, O_3, and OOF were also observed in the infrared spectra.[47]

In the reactions of cerium and 1.0% OF_2 in argon, product absorptions were observed at 849.4, 736.7, 793.9, 516.6, 487.5, 757.9, and 452.7 cm^{-1} (Figure 1 and Tables 1 and 2). The first two bands were previously assigned to the CeO^+ cation (849.4 cm^{-1} not shown)[9] as well as the antisymmetric O−Ce−O stretching mode of the CeO_2 molecule (736.7 cm^{-1}).[7,48,49] The new 793.9, 516.6, and 487.5 cm^{-1} absorptions increased when the sample was annealed to 20 K. All of the bands grew slightly upon broad band irradiation, and decreased during further sample annealing to 30 and 35 K. No obvious growth was observed for the 757.9 and 452.7 cm^{-1} bands although they sharpened during the first sample annealing. Additionally, one of the CeF_3 absorption appeared at 484 cm^{-1} (denoted by an *)[3,50] when the sample was annealed (the other CeF_3 band expected at 486 cm^{-1} was covered by the stronger 487.5 cm^{-1} band), and a band centered at 550 cm^{-1} was produced upon irradiation (λ > 220 nm), which was assigned to the CeF_4 molecule in earlier work[51] and our reaction of Ce with NF_3. The sharper band at 559 cm^{-1} may also be due to CeF_4 as it was also observed in our experiment with Ce and NF_3. Infrared spectra from the reactions of Ce and 1.0% $^{18}OF_2$/Ar mixture

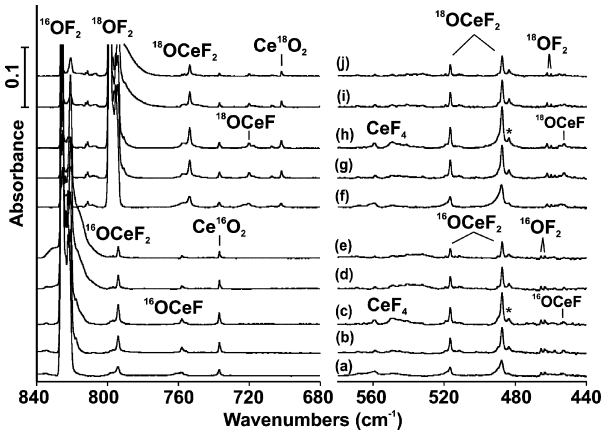

Figure 1. Infrared spectra of laser-ablated Ce atoms and OF_2 reaction products in solid argon: (a) Ce + 1.0% $^{16}OF_2$ deposition for 60 min; (b) after annealing to 20 K; (c) after λ > 220 nm irradiation; (d) after annealing to 30 K; (e) after annealing to 35 K; (f) Ce + 1.0% $^{18}OF_2$ deposition for 60 min; (g) after annealing to 20 K; (h) after λ > 220 nm irradiation; (i) after annealing to 30 K; (j) after annealing to 35 K. The asterisks denote the absorptions of CeF_3.

are shown in Figure 1, traces f−j. In addition to the $Ce^{18}O_2$ species, large ^{18}O shifts were observed for only two of the five new bands, which appeared at 720.0 and 753.6 cm^{-1}. A very small ^{18}O shift was observed for the 452.7 cm^{-1} band (0.2 cm^{-1}). The behavior of the product absorptions on annealing and photolysis are the same as those observed with the OF_2 sample.

The infrared spectra from the Ce and OF_2 reaction in a neon matrix are shown in Figure 2. The OF radical band exhibits a doublet at 1035.6 and 1031.2 cm^{-1}, and broad band irradiation favors the latter one. Common cerium oxide absorptions such as CeO^+ and CeO_2 were observed at 874.8 and 755.6 cm^{-1} (antisymmetric O−Ce−O str.) appropriately above the argon matrix bands.[52] The band centered at 552.7 cm^{-1} increased upon broad band irradiation and is the neon counterpart of the CeF_4 molecule. No change was found in the appearance of the CeF_3 band after sample deposition. In addition to these known products, new absorptions were observed at 808.4, 533.0, 504.1, and 778.9 cm^{-1}. Although the 778.9 cm^{-1} band almost remained unchanged throughout the experiments, the first three absorptions increased when the sample was irradiated by UV photons.

Similar to the cerium and OF_2 experiments, both Pr and Tb reacted with OF_2 to give two absorptions in the lower frequency region, which show almost no ^{18}O shift (Figure 3). For the third band in the higher frequency region, the Pr and Tb product bands were observed at 693.9 and 680.8 cm^{-1} respectively.

Figure 4 shows spectra from the Eu reaction, and EuF_2 bands are observed on deposition.[3,53] Four new absorptions were observed at 752.9, 532.7, 510.3, and 467.2 cm^{-1}, which increased slightly on annealing to 20 K and on >220 nm photolysis, and then decreased slightly on further annealing. These bands are distinguished by the large oxygen-18 shift for the higher band to 714.7 cm^{-1} (ratio 1.0534), which is near that for EuO at 667.8 cm^{-1} with the 1.0541 ratio.[5] As before the three lower bands exhibit small ^{18}O shifts.

The reaction of Yb and OF_2 in argon resulted in five new product absorptions at 516.3, 563.1, 546.1, 785.3, and 508.8 cm^{-1} (Figure 5). The first three bands increased during the first

dx.doi.org/10.1021/ic402422h | Inorg. Chem. 2014, 53, 446−456

Table 1. Infrared Absorptions (cm^{-1}) for the $OLnF_2$ and $^{18}OLnF_2$ Molecules in Solid Argon and Neon

				OF_2			$^{18}OF_2$			$^{16}O/^{18}O$			
Ln[a]	obs matrix or calc.	spin/ (S^2 theory)/ S^2	nominal "f occ"	Ln−O(I)[a]	sym. F−Ln(I)[a]	asym. F−Ln(I)[a]	Ln-^{18}O(I)[a]	sym. F−Ln (I)[a]	asym. F−Ln(I)[a]	Ln−O str	spin O	Ln oxid no.	ΔH(0 K) Rxn (1) kcal/mol
Ce	Ar			793.9	516.6	487.5	753.6	516.6	487.5	1.0535			
Ce	Ne			808.4	533.0	504.1							
Ce	B3LYP	1	f^0	843 (234)	533 (127)	507 (248)	799 (212)	533 (127)	507 (247)	1.0542	0	IV	−363.0
Pr	Ar			693.9	519.1	476.8	658.6	519.1	476.8	1.0536			
Pr	Ne			706.0	534.7	492.7	670.4	534.7	492.7	1.0531			
Pr	B3LYP	2 (0.75) 0.80	f^1	764 (177)	538 (138)	498 (224)	725 (163)	538 (136)	498 (224)	1.0544	−0.20	III/IV	−308.0
Nd	Ar				517.0	479.0		517.8	476.7				
Nd	B3LYP	5 (6.00) 6.01	f^3	518 (206)	542 (5)	532 (161)	496 (152)	537 (49)	531 (161)	1.0443	0.89	III	−295.2
Pm	B3LYP	4 (3.75) 3.77	f^4	487 (120)	545 (71)	527 (237)	463 (103)	544 (80)	527 (237)	1.0529	−1.01	III	−276.3
Pm	B3LYP	6 (8.75) 8.76	f^4	530 (203)	550 (0)	573 (77)	509 (157)	543 (37)	573 (76)	1.0407	0.89	III	−265.4
Sm	Ar				527.4	497.0[b]		527.7	496.5[b]				
Sm	Ne				542.1	518.7		543.0	518.3				
Sm	B3LYP	7(12.00) 12.01	f^5	504 (149)	551 (43)	549 (256)	479 (127)	550 (55)	549 (256)	1.0525	0.97	III	−246.1
Sm	B3LYP	5 (6.00) 6.96	f^5	502 (95)	545 (54)	538 (210)	477 (77)	544 (68)	538 (210)	1.0528	−0.95	III	−245.6
Eu	Ar				532.7	510.3		530.9	510.1				
Eu	B3LYP	6 (8.75) 9.79	f^6	492 (38)	552 (118)	462 (528)	466 (33)	552 (120)	462 (527)	1.0549	−1.03	III	−220.9
Eu	B3LYP	8(15.75) 15.79	f^6	533 (103)	554 (90)	484 (370)	505 (78)	554 (108)	484 (370)	1.0541	0.84	III	−218.8
Gd	Ar			499.0	537.8	517.8	474.3	536.7	517.8	1.0521			
Gd	B3LYP	9(20.00) 20.00	f^7	525 (129)	566 (41)	543 (203)	500 (107)	563 (55)	543 (203)	1.0507	0.98	III	−199.3
Tb	Ar			680.8	549.7	539.0	647.5	549.7	538.9	1.0514			
Tb	Ne				564.3	554.9							
Tb	BP86	8(15.75) 16.37	f^8/f^7	667 (42)	548 (67)	545 (162)	634 (35)	547 (70)	545 (162)	1.0525	0.65	III/IV	−302.0
Dy	Ar				548.4	530.5[c]		548.0	530.5[c]				
Dy	B3LYP	5 (6.00) 7.58	f^9	514 (135)	571 (49)	557 (192)	488 (116)	570 (59)	557 (192)	1.0528	−0.96	III	−326.7
Ho	Ar				549.1	529.1		548.7	529.3				
Ho	B3LYP	6 (8.75) 8.76	f^{10}	510 (118)	573 (55)	560 (184)	484 (102)	572 (62)	560 (184)	1.0537	0.99	III	−293.1
Er	Ar			517.7	556.1	539.0	492.3	555.4	539.0	1.0516			
Er	B3LYP	5 (6.00) 6.01	f^{11}	536 (111)	577 (46)	563 (190)	509 (93)	576 (57)	563 (189)	1.0535	0.99	III	−274.1
Tm	Ar			518.9	561.1	543.6	492.3	560.4	545.1	1.0540			
Tm	B3LYP	4 (3.75) 3.75	f^{12}	525 (116)	577 (45)	569 (182)	499 (98)	576 (56)	569 (181)	1.0534	1.00	III	−249.9
Yb	Ar			516.3	563.1	546.1	490.5	562.3	546.0	1.0526			
Yb	Ne			532.1	578.3	563.4	505.3	577.7	563.4	1.0530			
Yb	B3LYP	3(2.00) 2.00	f^{13}	544 (79)	578 (59)	570 (181)	515 (69)	578 (62)	570 (180)	1.0546	1.01	III	−232.9
Lu	Ar			532.3	566.7	552.1[c]	505.2	566.3	552.1[c]	1.0536			
Lu	Ne			549.4	581.4	569.1	521.4	581.2	569.1	1.0537			
Lu	B3LYP	2 (0.75) 0.75	f^{14}	550 (91)	581 (45)	571 (183)	521 (77)	580 (52)	571 (182)	1.0544	1.00	III	−310.6

[a]Infrared intensity I in km/mol in parentheses. [b]Major site absorption. [c]Overlapped with LnF_3 absorption.

dx.doi.org/10.1021/ic402422h | Inorg. Chem. 2014, 53, 446−456

Table 2. Infrared Absorptions (cm^{-1}) of the OLnF and ^{18}OLnF Molecules in Solid Argon and Neon

			OF		^{18}OF		^{16}O/^{18}O		
Ln[a]	observed matrix or calculated	spin/ (S^2 theory) /S^2	Ln−O str. (I)	Ln−F str. (I)	Ln−^{18}O str. (I)	Ln−F str. (I)	Ln−O str	spin O	ΔH(0 K) Rxn (2) kcal/mol
La	B3LYP	1	778	467	738	467	1.0539	0	−244.8
Ce	Ar		757.9	452.7	720.0	452.5	1.0526		
Ce	Ne		778.9						
Ce	B3LYP	2 (0.75) 0.75	790 (262)	478 (173)	749 (236)	478 (173)	1.0540	0	−245.1
Pr	Ar		767.5	451.2	728.2	451.2	1.0540		
Pr	Ne		787.8		747.8		1.0535		
Pr	B3LYP	3 (2.00) 2.01	794 (255)	502 (169)	753 (229)	502 (169)	1.0544	0	−208.5
Nd	Ar		768.1	457.6	729.2	457.2	1.0533		
Nd	B3LYP	4 (3.75) 3.79	793 (232)	479 (171)	753 (209)	479 (171)	1.0531	−0.15	−198.9
Pm	B3LYP	5 (6.00) 6.02	795 (231)	514 (162)	754 (207)	514 (162)	1.0544	−0.10	−186.3
Sm	Ar		769.9	469.5	730.6	469.3	1.0538		
Sm	B3LYP	6 (8.75) 8.81	767 (184)	503 (155)	727 (165)	503 (155)	1.0550	−0.18	−160.7
Eu	Ar		752.9	467.2	714.7	467.0	1.0534		
Eu	B3LYP	7 (12.00) 12.27	634 (66)	487 (151)	601 (58)	487 (151)	1.0549	−0.40	−139.7
Eu	CCSD(T)	7 (12.00)	786	491	745	491	1.0550		
Gd	Ar		774.7	484.5	735.2	484.5	1.0537		
Gd	B3LYP	8 (15.75) 16.12	698 (70)	531 (131)	663 (61)	530 (132)	1.0528	−0.31	−171.5
Gd	CCSD(T)	8 (15.75)	791	511	750	511	1.0547		
Tb	Ar		784.7	489.3	744.4	489.3	1.0541		
Tb	B3LYP	9 (20.00) 20.04	850 (197)	546 (142)	806 (176)	546 (142)	1.0546	0	
Tb	B3LYP[b]	7 (12.00) 12.83	833 (230)	543 (142)	790 (207)	543 (142)	1.0544	0	−288.4
Dy	Ar		785.7	487.1	746.5	487.0	1.0525		
Dy	B3LYP	8 (15.75) 15.79	844 (175)	545 (142)	800 (157)	545 (142)	1.0550	0.12	−221.7
Dy	B3LYP	6 (8.75) 9.38	587 (7)	531 (133)	558 (6)	530 (133)	1.0520	−0.44	−206.5
Ho	Ar		790.5	492.8	747.8	492.6	1.0571		
Ho	Ne		811.3	511.5	767.1	511.5 br	1.0576		
Ho	B3LYP	5 (6.00) 6.01	798 (164)	526 (139)	757 (147)	526 (139)	1.0542	0.15	−168.6
Er	Ar		790.5	507.6	749.8	507.4	1.0543		
Er	B3LYP	4 (3.75) 3.75	856 (161)	553 (109)	813 (146)	553 (108)	1.0529	0.03	−166.5
Tm	Ar		794.8	511.2	753.8	511.0	1.0544		
Tm	B3LYP	3 (2.00) 2.00	794 (133)	544 (129)	753 (118)	543 (129)	1.0544	0.10	−146.1
Yb	Ar		785.3	508.8	745.0	508.6	1.0541		
Yb	Ne		803.8		762.3		1.0544		
Yb	CCSD(T)	2 (0.75)	796	531	754	531	1.0557		
Yb	B3LYP	2 (0.75)[c]	746 (97)	530 (130)	706 (91)	531 (130)	1.0567	0.05	−128.0
Lu	Ar		794.9	523.7	753.8	523.5	1.0545		
Lu	B3LYP	1	816 (119)	551 (120)	773 (105)	551 (120)	1.0556	0	−198.5

[a]All calculations done at the B3LYP/DZVP2+ Stuttgart/segmented basis set level unless noted. Infrared intensity I in km/mol in parentheses. [b]The septet is 5.3 kcal/mol lower than the nonet. [c]Restricted open shell Kohn−Sham.

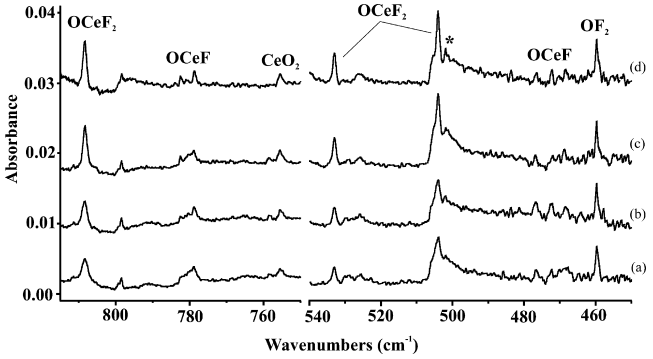

Figure 2. Infrared spectra of laser-ablated Ce atoms and OF_2 reaction products in solid neon: (a) Ce + 1.0% OF_2 deposition for 50 min; (b) after annealing to 8 K; (c) after λ > 220 nm irradiation; (d) after annealing to 10 K. The asterisk denotes an absorption of CeF_3.

sample annealing whereas no change was observed for the latter two bands. Broad band irradiation increased both sets of absorptions slightly, and they decreased upon further sample annealing to 30 and 35 K. Only the 516.3 and 785.3 cm^{-1} absorptions showed large ^{18}O shifts, to 490.5 and 745.0 cm^{-1}, while isotopic shifts for the other three bands are quite small. The absorptions due to YbF_2 were observed in both OF_2 and $^{18}OF_2$ reactions while the YbF_3 band was covered by the new band at 546.1 cm^{-1}.[3,55] Reactions of Gd, Er, Tm, and Lu with OF_2 gave similar product absorptions, which are summarized in Table 1 together with the other values.

$OLnF_2$ Experimental Assignments. In the cerium and OF_2 reaction, the 793.9, 516.6, and 487.5 cm^{-1} absorptions probably arise from the same molecule on their similar behavior on annealing and photolysis (Table 1). Experiments with $^{18}OF_2$ sample revealed that the first band shifted to 753.6 cm^{-1} while no isotopic shifts were observed for the latter two bands. Both the ^{16}O/^{18}O ratio (1.0535) and band position of the 793.9

dx.doi.org/10.1021/ic402422h | Inorg. Chem. 2014, 53, 446−456

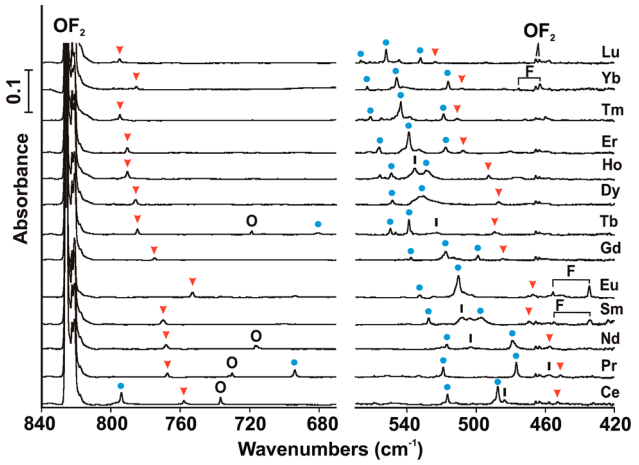

Figure 3. Infrared spectra of laser-ablated lanthanide atom and 1% OF_2 reaction products in solid argon at 4 K. All of the infrared spectra were recorded after annealing to 20 K following 1 h of sample deposition. Red triangle: OLnF; Blue dot: $OLnF_2$; Black bar: LnF_3 (this band is masked by the $OLnF_2$ band in the spectra without a black bar); O denotes LnO_2; F denotes LnF_2.

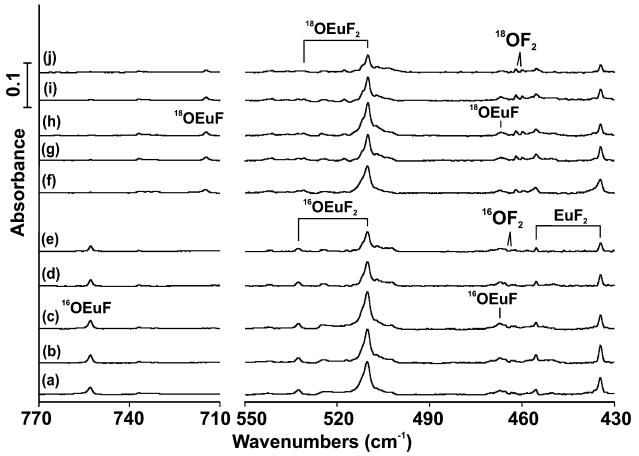

Figure 4. Infrared spectra of laser-ablated Eu atoms and OF_2 reaction products in solid argon: (a) Eu + 1.0% $^{16}OF_2$ deposition for 60 min; (b) after annealing to 20 K; (c) after $\lambda > 220$ nm irradiation; (d) after annealing to 30 K; (e) after annealing to 35 K; (f) Eu + 1.0% $^{18}OF_2$ deposition for 60 min; (g) after annealing to 20 K; (h) after $\lambda > 220$ nm irradiation; (i) after annealing to 30 K; (j) after annealing to 35 K.

cm^{-1} absorption are consistent with assignment of this band to the terminal Ce═O stretch of a new molecule. Furthermore, these values are close to those of diatomic CeO, which exhibits the ratio 1.0537 and absorbs at 808.3 cm^{-1} in solid argon.[9,49] The 516.6 and 487.5 cm^{-1} absorptions were observed in the region of Ce−F stretching absorptions, but these bands were not observed in previous experiments with NF_3. Hence we assign these two bands to the symmetric and antisymmetric F−Ce−F stretching modes of the new molecule, $OCeF_2$, which appears to be the major new product. The $OCeF_2$ molecule was also observed in solid neon at 808.4, 533.0, and 504.1 cm^{-1}, blue shifts of 14.5, 16.4, and 16.6 cm^{-1}, which are comparable to the shifts observed for CeF_3 and CeO_2 in this work. Following the cerium example, the $OPrF_2$ and $OTbF_2$ molecules can be identified with terminal Pr−O and Tb−O stretching vibrations of 693.9 and 680.8 cm^{-1}.

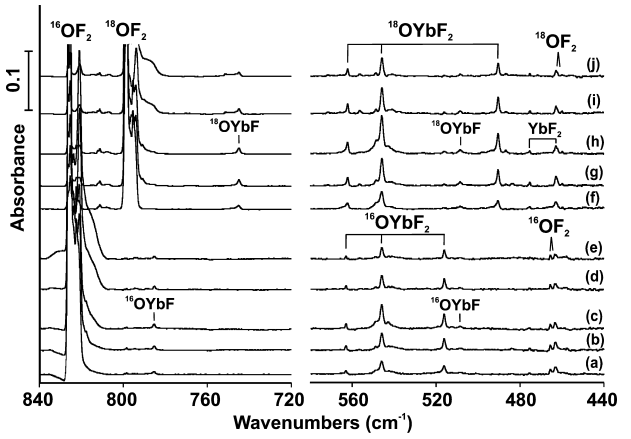

Figure 5. Infrared spectra of laser-ablated Yb atoms and OF_2 reaction products in solid argon: (a) Yb + 1.0% $^{16}OF_2$ deposition for 60 min; (b) after annealing to 20 K; (c) after $\lambda > 220$ nm irradiation; (d) after annealing to 30 K; (e) after annealing to 35 K; (f) Yb + 1.0% $^{18}OF_2$ deposition for 60 min; (g) after annealing to 20 K; (h) after $\lambda > 220$ nm irradiation; (i) after annealing to 30 K; (j) after annealing to 35 K.

The 516.3, 563.1, and 546.1 cm^{-1} absorptions observed in the Yb and OF_2 reactions shifted to 490.5, 562.3, and 546.0 cm^{-1} upon ^{18}O substitution (Table 1). The isotopic frequency ratio for the first band is 1.0526 in Ar and 1.0530 in Ne, close to the value of the YbO molecule itself (1.0547). Very small isotopic shifts of 0.8 and 0.1 cm^{-1} were observed for the weak band at 563.1 cm^{-1} and the strong band at 546.1 cm^{-1}, suggesting a very small amount of oxygen participation in these two modes. Thus, we assign these two new absorptions to the symmetric and antisymmetric F−Yb−F modes based on the band position and small ^{18}O shifts. With the observation of the three vibrational modes, the new Yb containing molecule should be $OYbF_2$. Similar sets of three absorptions around 500 cm^{-1} were observed for Gd, Er, Tm, and Lu reaction products with OF_2 as shown in Figure 3 and listed in Table 1. For the $OLnF_2$ molecules with Ln = Nd, Sm, Eu, Dy, and Ho, only two metal fluorine stretching modes were observed while no band with large ^{18}O shift was found to track both absorptions.

$OLnF_2$ Computational Assignments. The DFT calculations of the frequencies and energies in Table 1 are for the electronic ground states of the products. In a number of cases, it is difficult to assign the ground state. This arises because there is a choice in whether the Ln is in the IV, III, or a mixed III/IV state and for the III oxidation states if the singly occupied orbital on the O is high or low spin coupled to the Ln. In addition, the results can be dependent on the functional because of spin contamination. For Sm, the high spin coupled septet is essentially the same energy as the low spin coupled quintet and Ln−O and Ln−F stretches are very similar as well. For Eu, similar results are found with a larger difference in the Ln−O frequencies for the two states.

The calculated enthalpies at 0 K for the formation of the $OLnF_2$ ground state (Reaction 1) range from −199 kcal/mol for Gd to as high as −380 kcal/mol for Tb (Table 1). These calculations do not include spin orbit corrections, but in light of the size of the reaction energies, this neglect does not affect the result that these reactions are highly exothermic, nor does the fact that we have used DFT.

The Ln−F bond lengths decrease by 0.16 Å from the Ce to the Lu product, consistent with the lanthanide contraction (Table 3). The Ln−O bond distances clearly do not follow the

dx.doi.org/10.1021/ic402422h | Inorg. Chem. 2014, 53, 446−456

Table 3. Calculated Geometry Parameters for $OLnF_2$ Molecules[a]

Ln	spin	r(Ln−F)	r(Ln−O)	∠F−Ln−F	∠F−Ln−O	Δθ
Ce	1	2.091	1.794	110.5	117.9	13.8
Pr	2	2.082	1.802	101.8	127.5	3.2
Nd	5	2.083	2.041	119.8	120.1	0.0
Pm	4	2.065	2.133	117.7	116.0	10.3
Pm	6	2.069	2.052	121.3	119.3	0.0
Sm	5	2.062	2.009	122.6	118.7	0.0
Sm	7	2.057	2.159	127.0	116.5	0.0
Eu	6	2.049	2.035	102.0	129.0	0.0
Eu	8	2.046	2.053	104.2	127.9	0.0
Gd	9	2.025	2.119	115.7	108.3	27.3
Tb	8	2.017	1.903	119.8	107.9	2.8
Dy	5	2.006	2.108	118.8	114.3	12.7
Ho	6	2.005	2.101	117.7	112.5	17.4
Er	5	1.997	2.084	118.6	115.3	10.9
Tm	4	1.993	2.100	121.9	117.9	2.3
Yb	3	1.984	2.072	122.9	118.3	0.0
Lu	2	1.972	2.062	123.4	118.0	0.0
Hf	1	1.933	1.755	118.0	110.9	20.1

[a]Bond distances in Å. Bond angles in degrees. Calculated with the B3LYP functional, except Ln = Tb calculated with BP86.

lanthanide contraction. For the Ce and Pr products, the Ln−O bond lengths are near 1.8 Å. For Nd to Sm, the Ln−O bond lengths increase from 1.92 to 2.16 Å and decrease to 2.04 Å for Eu. The Ln−O bond length increases to 2.12 Å for Gd and decreases back to 1.90 Å for Tb. The Ln−O bond lengths increase to ∼2.10 Å for Dy and basically remain at this value decreasing by only 0.04 Å from Dy to Lu. The short Ln−O bond distance for $OCeF_2$ is due to Ce being in the IV oxidation state and for $OPrF_2$ as discussed in more detail below, the Pr is in the mixed II/IV oxidation state consistent with a short Pr−O bond. Similarly, the Tb in $OTbF_2$ is in a mixed III/IV oxidation state, and the bond length is again quite short.

About half of the $OLnF_2$ molecules are planar with C_{2v} symmetry and half are nonplanar with C_s symmetry. We represent the nonplanarity by the quantity $\Delta\theta$, which is the deviation of the sum of the bond angles around the metal from 360°. The deviation from planarity is not large. The molecules clearly in the IV oxidation state, $OCeF_2$ and $OHfF_2$, are slightly nonplanar. Except for $^4OPmF_2$ in the low spin coupling, the early III oxidation state $OLnF_2$ compounds are essentially planar. The most nonplanar compound is $OGdF_2$ in the high spin state. The deviation from planarity predicted for the later III oxidation state $OLnF_2$ compounds is small and approximately decreases as the f orbitals become fully occupied. The F−Ln−F angles do not exhibit any periodic pattern and range from 99° to 127°. There is more variation for the earlier lanthanides. The F−Ln−F angle for the later lanthanides starting at Gd increases by about 8° from 116°. The O−Ln−F angles do not exhibit any periodic pattern and range from 108° to 130°. Again, there is more variation of the early lanthanides. From Gd to Lu, the O−Ln−F bond angles increase by about 10° from 108°.

The assignments of the observed vibrational transitions to $OLnF_2$ molecules given above are supported by our electronic structure calculations at the DFT level as shown in Table 1. We note that care must be taken in the calculations, and the amount of spin density on O is important for determining the correct frequencies. The calculated Ln−O stretching frequencies range from 500 to 900 cm^{-1} and the $^{16}O/^{18}O$ stretching frequency ratios from 1.051 to 1.056, which corresponds to an ∼30 cm^{-1} difference for the heavy oxygen substitution for all of the lanthanides, except for Nd and Pm where the respective ratios are 1.049 and 1.041.

We first discuss the limiting case with f^0 occupancy and a IV oxidation state on the Ln. Frequency calculations on the $OCeF_2$ molecule give three infrared absorptions above 400 cm^{-1}. The terminal Ce═O mode is calculated at 843 cm^{-1} with the $^{16}O/^{18}O$ ratio of 1.0543, both in good agreement with the observed values. For the symmetric and antisymmetric F−Ce−F stretching modes, almost no isotopic shifts are predicted theoretically, consistent with the experimental results. Similar results are found for the $OPrF_2$ and $OTbF_2$ molecules with a high value for the Ln−O stretch as compared to the Ln−F stretches.

We next describe the limiting case of the $OLuF_2$ molecule with an f^{14} occupancy and a III oxidation state on the Ln. The calculations predict three similar vibrational frequencies at 550, 581, and 571 cm^{-1}. The latter two are the symmetric and antisymmetric F−Lu−F stretching modes with the former being weaker than the latter. Very small isotopic shifts are predicted for these two modes upon ^{18}O substitution, in agreement with the experimental observations. The calculated band at 550 cm^{-1} has a larger $^{16}O/^{18}O$ ratio of 1.0563, consistent with the observed isotopic shift for the experimental band and the value in the Ne matrix. Consistent with the results for $OLuF_2$, the three stretching vibrational frequencies of the Ln = Nd, Pm, Sm, Eu, Gd, Dy, Ho, Er, Tm, Yb molecules are in the range of ∼500 to ∼575 cm^{-1} with the Ln−O stretching vibration being the lowest. Both the isotopic shifts and the band positions for these products calculated at the B3LYP level fit the experimental results well.

The most important electronic structure properties for $OLnF_2$ are the formal oxidation state of the metal and the oxygen, both of which affect the Ln−O bond. The oxidation state of the F is formally −1 and does not change, consistent with the fact that the Ln−F stretches do not exhibit the large variation found for the Ln−O stretching modes. Thus, the Ln−F bond can be considered to be ionic with an F^- interacting with a positively charged Ln. This is consistent with the variation in the Ln−F bond distances which follow the expected lanthanide contraction and the corresponding changes in the Ln−F stretches. Because, the F is more electronegative than the oxygen, it will remain with a formal −1 charge and if the oxidation state on an anionic ligand has to change, this will happen on the oxygen.

The variation in the Ln−O stretches as compared to the smaller variation in the Ln−F stretches occurs because the Ln can be in different oxidation states, either III or IV (or a mixed III/IV state), and the variation in oxidation state on the Ln results in the oxidation state on the O being −1 or −2. If the Ln is in the IV oxidation state, then the O is in the −2 oxidation state and, as O^{2-} is closed shell, we expect to find little spin density on the O. The spin densities are shown in Figure 6. If the Ln is in the III oxidation state, then the O should have an excess spin. This spin can either be in the same spin orientation (α) or opposite (spin polarized β). When the Ln is in the IV oxidation state, then the Ln−O stretch should be at a higher frequency as the ionic interaction is larger, namely, a +2 charge on the cation (2 charges are already balanced by the two F^-) interacting with a −2 oxygen anion. When the Ln is in the III oxidation state, the Ln−O frequency should be lower as it is a

dx.doi.org/10.1021/ic402422h | Inorg. Chem. 2014, 53, 446−456

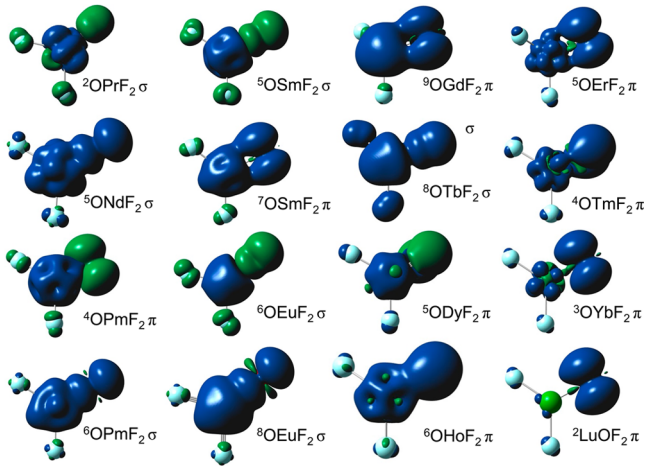

Figure 6. Spin densities for OLnF$_2$ at the 0.0015 contour level. Blue = positive spin density and green = negative spin density. Significant amounts of negative spin show spin polarization. The σ and π correspond to the excess spin density on the O in terms of its interaction with the Ln.

+1 charge on the cation interacting with a −1 charge on the O, both assuming full ionicity in the Ln−F bonds.

For OCeF$_2$, the Ce is in the IV oxidation state, and the Ce−O frequency has the largest value. For OPrF$_2$, there is a single f electron in oxidation state IV and some spin delocalization to the O (−0.20 e) occurs. Thus, the Pr is in a mixed III/IV oxidation state, and the Pr−O stretch decreases by ∼100 cm^{-1} as compared to the Ce−O value with the IV being dominant. Nd has the possibility of f^3 occupancy in oxidation state III or f^2 occupancy in oxidation state IV. The experimental Nd−O stretch was not observed, but we do predict that the Nd is clearly in the III oxidation state with a much lower Nd−O frequency as compared to OCeF$_2$ and OPrF$_2$. The B3LYP functional for the mixed III/IV state predicts a Nd−O stretch that is very low, ∼ 420 cm^{-1}, and the BP86 functional predicts one that is high, ∼ 660 cm^{-1}. Neither frequency was observed, so we can eliminate the presence of the mixed III/IV state for ONdF$_2$. OPmF$_2$ cannot be readily studied experimentally, and we note that the calculations predict the Pm to be in the III oxidation state. For OSmF$_2$, the Sm is clearly in the III oxidation state with the high spin coupling of the spin on the O with the Sm giving the more stable state. In this case the difference in the frequencies of the high and low spin coupled states is small as noted above. OEuF$_2$ and OGdF$_2$ remain in the III oxidation state with Ln−O stretches around 500 cm^{-1} as the f shell is being filled one electron at a time. For OTbF$_2$, as noted above, there is a large amount of symmetry breaking with the B3LYP functional, so we used the generalized gradient functional BP86 with no component of Hartree−Fock exchange. The analysis of the results shows that the nominally stable f^7 occupancy is not found but that ∼0.65e is transferred to the O to give a mixed oxidation III/IV state and a larger frequency near 700 cm^{-1}, comparable to the value for OPrF$_2$, exactly as observed from the experiment. The oxidation state returns to III for the remaining Ln from Dy to Lu as the f orbitals become doubly occupied. For ODyF$_2$, the expected high spin structure has S^2 = 12.50 (as compared to a predicted value of 12.00) and is 13 kcal/mol less stable than the low spin coupled structure. In addition, the high spin structure has the Ln in the III/IV oxidation state with a predicted Dy−O frequency of 688 cm^{-1}. There is no such frequency observed in the experimental spectrum so this state is not present. The low spin coupled state has a Dy−O frequency of ∼515 cm^{-1} consistent with what is expected for an Ln in the III oxidation state. The Ln−O frequencies only increase from ∼510 cm^{-1} to ∼550 cm^{-1} for the remaining Ln, consistent with the fact that the Ln−O bond decreases by about 0.04 Å in this range. The changes in the Ln−O and Ln−F bond distances and frequencies for the heavier lanthanides are consistent with the lanthanide contraction. For these heavier lanthanides, there is essentially a pure spin on the O, and this spin is high spin coupled with the f orbitals on the Ln except for Dy where it is low spin coupled.

OLnF Experimental Assignments. We describe the results for the Ce + OF$_2$ reaction as an example (Table 2). The two absorptions observed at 757.9 and 452.7 cm^{-1} in the Ce and OF$_2$ reactions are due to another new molecule different from OCeF$_2$. The first band shifted to 720.0 cm^{-1} upon ^{18}O substitution. The ^{16}O/^{18}O isotopic ratio of 1.0526 characterizes a Ce−O stretching mode, and the band position supports the assignment of a terminal mode. For the other band at 452.7 cm^{-1}, the ^{18}OF$_2$ sample gave a band almost the same as the one observed in the ^{16}OF$_2$ experiment. Both the band position and the negligible ^{16}O/^{18}O isotopic shifts indicate a Ce−F stretching vibrational mode for this low frequency band. Hence the second new molecule produced in the Ce and OF$_2$ reactions is identified as OCeF. Note that the 757.9 cm^{-1} absorption is very close to the symmetric O−Ce−O mode of the cerium dioxide molecule at 757.3 cm^{-1}. However, the symmetric mode is much weaker than the antisymmetric mode, and the new band at 752.9 cm^{-1} is in a similar position as the symmetric O−Ce−O mode for CeO$_2$. The OCeF molecule was also observed in solid neon where the two bands were split by the matrix: the major site absorptions were 778.9 and 472.5 cm^{-1}. These bands were blue-shifted in solid neon 20.9 and 19.8 cm^{-1} from the solid argon values, which are comparable to the matrix shifts for other molecules such as CeF$_3$ and OThF$_2$.[3,24,50] The OLnF molecules are observed for all of the lanthanide metals, and they are characterized by terminal Ln−O and Ln−F stretching vibrations. The Ln−O bands were found in the 700−800 cm^{-1} region for all of these products, while the Ln−F bands for some product molecules were not observed because of their weak intensities.

OLnF Computational Assignments. The reaction enthalpies at 0 K for the formation of the ground state of OLnF (Reaction 2), range from −128 kcal/mol for Yb to −288 kcal/mol for Tb (Table 2). The expected oxidation state of the Ln is III in all cases with a nominal oxidation state of −1 on F and −2 on O in the fully ionic model. The reaction energies become less exothermic as the metal 4f orbitals are individually filled from Ce to Eu. For Gd, the f-shell is half full with one electron in a d orbital, and the reaction energy increases to −172 kcal/mol from the value of −140 kcal/mol for Eu. For Tb the reaction energy is the most exothermic for the entire series. As the f orbitals become doubly occupied, the reaction energy again decreases from Tb to Yb. The f shell is completely full for Lu, and the reaction energy is about −200 kcal/mol. There is substantial spin delocalization to the oxygen for Eu, Gd, and Yb at the DFT/B3LYP level. The spin densities are shown in Figure 7. The Ln−O frequencies become too low so we used R/UCCSD(T) with the aug-cc-pVDZ basis set on O and F and the ECP28MWB segmented basis set for the lanthanides for these 3 molecules.

dx.doi.org/10.1021/ic402422h | Inorg. Chem. 2014, 53, 446−456

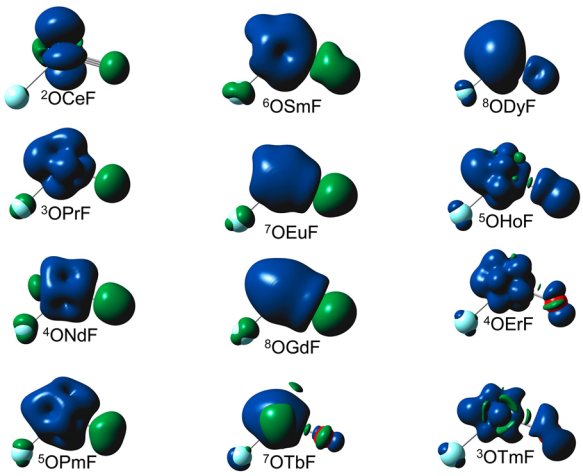

Figure 7. Spin densities for OLnF at the 0.0015 contour level. Blue = positive spin density and green = negative spin density. Significant amounts of negative spin show spin polarization.

The OLnF products are all bent with bond angles in the range of 110° to 126° (Table 4) and do not exhibit any periodicity. The Ln−F bond lengths decrease by 0.16 Å from Ce to Lu, essentially following the Ln contraction. The Ln−O bond distances have a much smaller range of values and only follow the lanthanide contraction qualitatively. The OLnF angle ranges over ∼15° and does not really exhibit any periodic behavior.

Table 4. Calculated Geometry Parameters for OLnF Molecules[a]

Ln	method	spin	r(Ln−F)	r(Ln−O)	∠F−Ln−O
Ce	B3LYP	2	2.150	1.844	119.2
Pr	B3LYP	3	2.122	1.836	114.1
Nd	B3LYP	4	2.137	1.820	122.4
Pm	B3LYP	5	2.107	1.831	113.7
Sm	B3LYP	6	2.108	1.832	118.6
Eu	B3LYP	7	2.111	1.862	124.4
Eu	CCSD(T)	7	2.114	1.822	117.9
Gd	B3LYP	8	2.059	1.880	105.4
Gd	CCSD(T)	8	2.077	1.826	110.0
Tb	B3LYP	7	2.045	1.807	114.1
Tb	B3LYP	9	2.044	1.798	117.5
Dy	B3LYP	8	2.033	1.788	120.3
Ho	B3LYP	5	2.058	1.816	119.6
Er	B3LYP	4	2.029	1.824	114.8
Tm	B3LYP	3	2.026	1.822	117.7
Yb	B3LYP[b]	2	2.017	1.838	123.2
Yb	CCSD(T)	2	2.029	1.813	125.7
Lu	B3LYP	1	1.989	1.815	112.3

[a]Bond distances in Å. Bond angles in degrees. [b]Calculated with MOLPRO version of B3LYP.

The calculated OLnF bending modes are between 150 to 200 cm^{-1} and are not further discussed as they are below our spectral limit. As an example for the Ln−O assignments, the Ce−O stretching mode for OCeF is calculated to be 790 cm^{-1} with an $^{16}O/^{18}O$ isotopic ratio of 1.0540, consistent with the value of 758 cm^{-1} observed in the argon matrix with an isotopic ratio of 1.0526. The Ce−F stretch is calculated at 478 cm^{-1} consistent with the experimental band at 453 cm^{-1} when the effect of a matrix shift is considered. The calculated Ln−O stretching frequencies range from 750 to 850 cm^{-1} as compared to the experimental range of 750−790 cm^{-1}. The higher Ln−O frequencies are predicted for the heavier metals with Tb, Dy, and Er having the highest M−O frequencies between 833 and 856 cm^{-1}, consistent with the shorter Ln−O bonds expected for the lanthanide contraction. For ODyF, the Dy−O stretching frequency of the more stable high spin state is consistent with experiment whereas the less stable lower spin state has a low frequency with significant spin polarization on the O. The Dy in ODyF has a formal s^1f^8 occupancy. The lighter lanthanides have a lower calculated oxygen stretch frequency of about 790 cm^{-1}. The $^{16}O/^{18}O$ isotopic ratios of 1.052−1.057 for the Ln−O stretching frequency are consistent with the experimental values for all metals. The Ln−F stretches also follow the lanthanide contraction, increasing with atomic number consistent with the decrease in the Ln−F bond distance.

Bonding in $OLnF_2$ and OLnF. The lanthanide metals are mostly in the III or IV oxidation state for the $OLnF_2$, except for $OPrF_2$ and $OTbF_2$ which are in a mixed III/IV state, and in the III oxidation state for OLnF. We first discuss the bonding for Ln(IV) as exemplified by $OCeF_2$, the only $OLnF_2$ in the pure IV oxidation state. These results are consistent with the known ability of Ce, Pr, and Tb (and only these three lanthanides) to form the tetrahalides CeF_4, PrF_4, and TbF_4.[54] As discussed above, the Ln−F bond is quite ionic, and the bond length follows the lanthanide contraction. The Ce−F bond has only 8% Ce character from a Natural Bond Orbital (NBO) analysis (Table 5).[55−58] The simplest description of the bonding for the Ln−O bond would be that it is ionic as well with an O^{2-}. In terms of the molecular orbitals (Figure 8), the Ln−O bonding can be described by a polarized σ bond and two pseudo π bonds formed by donation from the two 2p lone pairs on the O to the Ce. The NBO analysis provides additional useful information about the character of the Ce−O bond. The polarized σ bond has 24% character on Ce split between 5d and 4f. The pseudo π bonds have 16−17% Ce character, again in the 5d and 4f orbitals. On the O, the pseudo π bonds have 100% p character and the polarized σ bond has 89% 2p character. Overall, there is about 1 electron in the 4f orbitals and about one electron in the 5d orbitals. At the end of the Ln block is $OHfF_2$. The bonding between the Hf−F and Hf−O is even more ionic than in $OCeF_2$ (Table 5). As the 4f orbitals are filled, the 6s, 6p, and 5d orbitals have electron density on the metal with the 5d being the most important.[23] Thus the $OCeF_2$ in the IV oxidation state is similar in some respects to $OHfF_2$, but differs in other aspects because of the availability of the 4f orbitals in the former. The results in Table 6 show that there is very little population in the 6s except for spin polarization in $OTbF_2$ and $ODyF_2$ and (not shown), about 0.03 to 0.08 electrons in the 6p orbitals. Thus the 6s and 6p orbitals are generally not involved in any bonding. In general, there are 0.6 to 1.0 electrons in the 5d orbitals on the Ln with a limit of 1.6 electrons on the Hf.

The Ln−O stretching frequencies for $OPrF_2$ and $OTbF_2$ show that the Ln have a mixed III/IV oxidation state with a lower Ln−O frequency than in $OCeF_2$, but with Ln−O stretches which are substantially larger than the Ln−O stretches of the remaining compounds. The NBO analysis for $OPrF_2$ and $OTbF_2$ (Table 6 and Supporting Information) shows substantial spin polarization with different types of bonds for the α and β spins. Only one Tb−O bond for the α spin but 3 Tb−O bonds for the β spin electrons are found in the NBO

dx.doi.org/10.1021/ic402422h | Inorg. Chem. 2014, 53, 446−456

Table 5. Calculated B3LYP NBO Analysis for $OCeF_2$, $OHfF_2$, OLaF, OLuF, and OCeF

bond	M pop %	M(%6s)	M(%5d)	M(%4f)	F/O pop%	F/O(%2s)	F/O(%2p)
				$OCeF_2$			
Ce−F	8		58	38	92	23	77
Ce−O π	17		53	46	83		100
Ce−O π	16		38	61	84		100
Ce−O σ	27		46	52	73	11	89
				$OHfF_2$			
Hf−F Flp	5	11(18p)	69		95		100
Hf−F σ	8	16(30p)	53		92	31	69
Hf−O π	19	11(10p)	78		81		97
Hf−O σ	18	9	90		82	17	83
Hf−O π	13	30p	68		87		100
				OLaF			
La−F	6		71	25	94	20	80
La−O π	13		80	19	87		100
La−O π	12		70	27	88		100
La−O σ	21		70	23	79	11	89
				OLuF			
Lu−F	6	27		69	94	25	75
Lu−O π	13			96	87		100
Lu−O π+ σ	16	18	74		84	5	95
Lu−O π+ σ	11		91		89	8	92
				OCeF(α)			
Ce−O π	14		75	25	86		100
Ce−O π	14		67	30	86		100
Ce−O σ	22		67	29	78	10	90

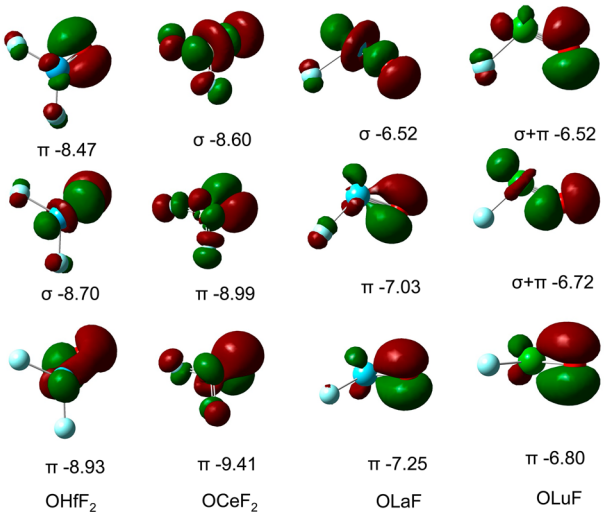

Figure 8. Molecular orbitals for closed shell $OHfF_2$, $OCeF_2$, OLaF, and OLuF at the 0.05 contour level. Orbital energies in eV.

Table 6. Calculated Total B3LYP NBO Analysis for $OLnF_2$[a]

Ln	spin	6sα	6sβ	4fα	4fβ	5dα	5dβ
Ce	1	0.03		0.92		1.04	
Pr	2	0.02	0.02	1.65	0.41	0.47	0.46
Nd	3	0.01	0.01	3.10	0.10	0.34	0.30
Pm	4	0.01	0.01	4.07	0.08	0.36	0.30
Pm	6	0.01	0.01	4.09	0.09	0.35	0.30
Sm	5	0.01	0.01	5.09	0.09	0.35	0.31
Sm	7	0.02	0.01	5.06	0.07	0.33	0.30
Eu	8	0.01	0.01	6.11	0.07	0.34	0.28
Eu	6	0.01	0.01	6.15	0.07	0.33	0.28
Gd	9	0.06	0.05	6.99	0.05	0.36	0.31
Tb	8	0.01	0.62	6.99	0.35	0.52	0.43
Dy	5	0.01	0.60	6.99	1.53	0.32	0.30
Ho	6	0.03	0.03	7.00	3.05	0.33	0.30
Er	5	0.03	0.03	7.00	4.04	0.32	0.31
Tm	4	0.03	0.03	7.00	5.05	0.29	0.27
Yb	3	0.03	0.03	7.00	6.02	0.29	0.30
Lu	2	0.04	0.04	7.00	7.00	0.33	0.33
Hf	1					1.57	

[a] α and β correspond to the two types of unpaired spins.

analysis. In fact, one of the Tb−O β spin orbitals has 58% on Tb and 42% on O with 63% 6s character on the Tb and smaller amounts in the 5d and 4f orbitals. For the total populations for $OTbF_2$, there is substantial spin polarization with 0.6 β electrons in the 6p and 0.4 β electrons in the 4f. There is also a larger 5d orbital population than in most of the remaining lanthanides of about 1 electron. For $OPrF_2$, there is less spin polarization with the NBOs for the α and β spins having similar character. For $OPrF_2$ (Table 6), there are about two electrons in the 4f orbitals (1.6 α and 0.4 β) and just less than one electron in the 5d orbitals (equal contributions from α and β spins).

The bonding for the $OLnF_2$ compounds in the III oxidation state is predicted to be very ionic in terms of the NBO analysis as exemplified by $OGdF_2$ and $OHoF_2$. The O is in the −1 oxidation state giving a longer bond, lower Ln−O stretching frequencies, and a spin on the O. Thus the bonding for $OLnF_2$ with the Ln in the III oxidation state resembles the bonding in H_2CLnF_2, where there is only a Ln−C σ bond which is highly polarized to the C (85%) and a single electron in the out-of-plane p orbital on the C.[3] As the O is more electronegative than the CH_2 group, the σ bond is even more polarized in $OLnF_2$ leading to the fully ionic NBO analysis. It is useful to note that

dx.doi.org/10.1021/ic402422h | Inorg. Chem. 2014, 53, 446−456

both the O and the CH_2 have triplet ground states to support this type of bonding for the III oxidation state of the lanthanides. The predominance of the III oxidation state except for the three lanthanides described above is consistent with the known chemistry of the lanthanides.[54] The total orbital NBO populations in Table 6 show that only Dy (and Pr and Tb as discussed above) have significant spin polarization in the 4f orbitals. In the III oxidation state lanthanides, there are about 0.6 electrons in the 5d orbitals.

The bonding in OLnF is determined by the fact that the formal oxidation state on the Ln is always III. The Ln−F bond is still a very ionic bond. The Ln−O bond in OLnF does not exhibit the same trends in the bond distances as in $OLnF_2$ yet it also does not follow the lanthanide contraction as do the Ln−F bonds. Again, the Ln−O bond can first be considered as fully ionic and it is more ionic than the Ce−O bond in $OCeF_2$ as shown by the OLaF and OLuF orbitals (Figure 8). This is probably the reason for the larger argon to neon blue shift for the Ln−O stretching modes in the OLnF molecules as compared to their $OLnF_2$ analogues. In the Ce case, these blue shifts are 20.9 and 14.5 cm^{-1}, respectively. For Pr these shifts are 20.3 and 12.1 cm^{-1} and for Y 18.5 and 15.8 cm^{-1} (Tables 1 and 2). The NBO analysis (Table 5) again shows a polarized Ln−O σ bond and two pseudo π bonds formed by donation from the two 2p lone pairs on the O to the Ln. In OLaF, donation to the metal is mostly to the 5d orbitals with about 25% into the 4f orbitals. In OLuF, the σ and in-plane π orbitals mix and the electrons on the O donate mostly into the empty 5d orbital. The out-of-plane π bond contribution on the metal is essentially all in the 4f orbitals. The orbitals for OCeF on the metal are again dominated by the 5d with some 4f contribution as in OLaF.

The NBO orbital populations in OLnF (Table 7) exhibit results similar to those for $OLnF_2$. The 6s orbitals are not

Table 7. Calculated Total B3LYP NBO Analysis for OLnF[a]

Ln	spin	6sα	6sβ	4fα	4fβ	5dα	5dβ
La	1	0.02		0.26		0.93	
Ce	2	0.01	0.01	1.15	0.15	0.48	0.45
Pr	3	0.01	0.01	2.13	0.15	0.52	0.44
Nd	4	0.01	0.01	3.25	0.14	0.45	0.41
Pm	5	0.01	0.01	4.12	0.13	0.52	0.42
Sm	6	0.01	0.01	5.18	0.11	0.49	0.39
Eu	7	0.01	0.01	6.02	0.03	0.47	0.33
Gd	8	0.01	0.01	6.99	0.03	0.51	0.33
Tb	7	0.01	0.79	6.99	0.37	0.57	0.46
Dy	8	0.90	0.01	6.99	1.3	0.65	0.4
Ho	5	0.02	0.02	6.99	3.25	0.45	0.38
Er	4	0.02	0.02	6.99	4.08	0.48	0.44
Tm	3	0.02	0.02	6.99	5.13	0.44	0.42
Yb	2	0.02	0.02	6.99	6.50	0.34	0.32
Lu	1	−0.09		0		0.94	

[a] α and β correspond to the two types of unpaired spins.

populated except for spin polarized OTbF and ODyF. ODyF has a high spin state with an open shell on the 6s, giving a formal s^1f^8 occupancy. The total 6p population is again in the range of 0.06 to 0.09 electrons. Except for OTbF, OHoF, ODyF, and OYbF, there is not much spin polarization in the 5f orbitals. There is a larger contribution of the 5d orbitals in the bonding with about 1 electron in these orbitals across the series.

CONCLUSIONS

Laser-ablated lanthanide metal atoms were condensed with OF_2 in excess argon or neon at 4 K. New infrared absorption bands are assigned to the oxidative addition products $OLnF_2$ and OLnF on the basis of ^{18}O isotopic substitution and electronic structure calculations of the vibrational frequencies. Two products, $OLnF_2$ and OLnF, were observed in the matrix. The dominant absorptions in the 500 cm^{-1} region are identified as lanthanide-fluoride stretching modes, consistent with other $XLnF_2$ structures. The Ln−F stretches effectively follow the lanthanide contraction, the Ln−F bonds are highly ionic, and the F can be considered to be in the −1 oxidation state. $OCeF_2$, $OPrF_2$, and $OTbF_2$ have higher frequency Ln−O stretches. The Ce═O stretch is the highest and the Ce is assigned to the IV oxidation state with the O in the −2 oxidation state. The Pr═O and Tb═O stretches are about 100 cm^{-1} lower, so the Pr and Tb are assigned to the mixed III/IV oxidation so the oxidation state for the O is between the −2 and −1. The remaining $OLnF_2$ compounds have the Ln in the III oxidation state as do all of the OLnF compounds. The O in the $OLnF_2$ compounds in the III oxidation state is in the −1 oxidation state which means that there is effectively a spin on the O.

The electronic structure calculations have to be done carefully because of issues with spin polarization. Significant fractional spin on the O can lead to issues in assigning the ground state as well as the oxidation state on the metal. The Ln−O stretching frequency is a good benchmark against which to test the computational results as it is very sensitive to the calculation and the amount of spin polarization. For $OLnF_2$ with the early lanthanides with the Ln in the III oxidation state, the spin on the O can be coupled either high spin or low spin with the Ln. For the latter lanthanides with the Ln in the III oxidation state, the spin on the O is mostly coupled high spin with the spin on the Ln. In $OCeF_2$, the bonding between Ce and O is best described as a highly polarized σ bond and two pseudo π bonds formed by donation from the two 2p lone pairs on the O to the Ce. The 5d and 4f orbitals on the Ce are those involved in the bonding between Ce and O. The Ln−O bonds in $OPrF_2$ and $OTbF_2$ show substantial spin polarization with some s character involved in the Tb−O bonding. The bonding for the $OLnF_2$ compounds in the III oxidation state is predicted to be fully ionic even though the O is in the −1 oxidation state.

In OLnF, there is essentially no spin on the oxygen as the Ln is in the III oxidation state so the O is in the −2 formal oxidation state and the F is in the formal −1 oxidation state. The analysis of the bonding in OLnF shows that the Ln−F bond is still very ionic. The Ln−O bonds in OLaF and OLuF are more ionic than the Ce−O bond in $OCeF_2$ and can be described by the same bonding scheme of a highly polarized σ bond and two pseudo π bonds. The La−O bonding is dominated by 5d orbitals on the La, and the Lu−O bonding has both 5d and 4f orbitals involved on the Lu. Thus, the bonding in $OLnF_2$ and OLnF is dominated by the oxidation state on the lanthanide and the Ln−O stretching frequency is an important measure of the oxidation state on the Ln and the spin state of the complex. The observation of larger neon to argon matrix shifts for several O−LnF modes as compared to their $O-LnF_2$ analogues is indicative of stronger matrix interaction through increased ionic character in the O−Ln bond in the OLnF species.

dx.doi.org/10.1021/ic402422h | Inorg. Chem. 2014, 53, 446−456

■ ASSOCIATED CONTENT

Supporting Information

Complete reference 34. NBO Analysis for $OPrF_2$ and $OTbF_2$. Total energies in a.u. Cartesian *x*, *y*, *z* coordinates in Å. This material is available free of charge via the Internet at http://pubs.acs.org.

■ AUTHOR INFORMATION

Corresponding Authors

*E-mail: dadixon@bama.ua.edu (D.A.D.).
*E-mail: lsa@virginia.edu (L.A.)

Notes

The authors declare no competing financial interest.

■ ACKNOWLEDGMENTS

We gratefully acknowledge financial support from the BES program in actinide sciences SISGR program (D.A.D. through Argonne National Laboratory), DE-SC0001034 (L.A) and DE-FG02-12ER16329 (K.A.P.). D.A.D. thanks the Robert Ramsay Fund at the University of Alabama and Argonne National Laboratory for partial support.

■ REFERENCES

(1) Hayton, T. W. *Chem. Commun.* **2013**, *49*, 2956−2973.
(2) Chen, M.; Dixon, D. A.; Wang, X.; Cho, H.-G.; Andrews, L. *J. Phys. Chem. A* **2011**, *115*, 5609−5624.
(3) Wang, X.; Cho, H.-G.; Andrews, L.; Chen, M.; Dixon, D. A.; Hu, H.-S.; Li, J. *J. Phys. Chem. A* **2011**, *115*, 1913−1921.
(4) Gong, Y.; Wang, X.; Andrews, L.; Chen, M.; Dixon, D. A. *Organometallics* **2011**, *30*, 4443−4452.
(5) Gong, Y.; Andrews, L.; Chen, M.; Dixon, D. A. *J. Phys. Chem. A* **2011**, *115*, 14581−14592.
(6) Willson, S. P.; Andrews, L. *J. Phys. Chem. A* **1999**, *103*, 3171−3183.
(7) Willson, S. P.; Andrews, L. *J. Phys. Chem. A* **1999**, *103*, 6972−6983.
(8) Willson, S. P.; Andrews, L. *J. Phys. Chem. A* **2000**, *104*, 1640−1647.
(9) Willson, S. P.; Andrews, L. *J. Phys. Chem. A* **1999**, *103*, 1311−1321.
(10) Willson, S. P.; Andrews, L. *J. Phys. Chem. A* **1998**, *102*, 10238−10249.
(11) Willson, S. P.; Andrews, L.; Neurock, M. *J. Phys. Chem. A* **2000**, *104*, 3446−3456.
(12) Wang, X. F.; Andrews, L.; Infante, I.; Gagliardi, L. *J. Phys. Chem. A* **2009**, *113*, 12566−12572.
(13) Infante, I.; Gagliardi, L.; Wang, X. F.; Andrews, L. *J. Phys. Chem. A* **2009**, *113*, 2446−2455.
(14) Zhou, M. F.; Jin, X.; Li, J. *J. Phys. Chem. A* **2006**, *110*, 10206−10211.
(15) Jin, X.; Jiang, L.; Xu, Q.; Zhou, M. F. *J. Phys. Chem. A* **2006**, *110*, 12585−12591.
(16) Jiang, L.; Jin, X.; Zhou, M. F.; Xu, Q. *J. Phys. Chem. A* **2008**, *112*, 3627−3630.
(17) Xu, J.; Jin, X.; Zhou, M. F. *J. Phys. Chem. A* **2007**, *111*, 7105−7111.
(18) Xu, J.; Zhou, M. F. *J. Phys. Chem. A* **2006**, *110*, 10575−10582.
(19) Jiang, L.; Xu, Q. *J. Phys. Chem. A* **2009**, *113*, 3121−3126.
(20) Jiang, L.; Xu, Q. *J. Phys. Chem. A* **2008**, *112*, 8690−8696.
(21) Jiang, L.; Zhang, X. B.; Han, S.; Xu, Q. *Inorg. Chem.* **2008**, *47*, 4826−4831.
(22) Gong, Y.; Andrews, L.; Bauschlicher, C. A., Jr. *J. Phys. Chem. A* **2012**, *116*, 10115−10121.
(23) Gong, Y.; Andrews, L.; Bauschlicher, C. A., Jr.; Thanthiriwatte, K. S.; Dixon, D. A. *Dalton Trans* **2012**, *41*, 11706−11715.
(24) Gong, Y.; Wang, X. F.; Andrews, L.; Schlöder, T.; Riedel, S. *Inorg.Chem.* **2012**, *51*, 6983−6991.
(25) Andrews, L.; Citra, A. *Chem. Rev.* **2002**, *102*, 885−911.
(26) Andrews, L. *Chem. Soc. Rev.* **2004**, *33*, 123−132.
(27) Andrews, L.; Cho, H.-G. *Organometallics* **2006**, *25*, 4040−4053.
(28) Arkell, A. *J. Am. Chem. Soc.* **1965**, *87*, 4057−4062.
(29) Becke, A. D. *J. Chem. Phys.* **1993**, *98*, 5648−5652.
(30) Lee, C.; Yang, W.; Parr, R. G. *Phys. Rev. B* **1988**, *37*, 785−789.
(31) Godbout, N.; Salahub, D. R.; Andzelm, J.; Wimmer, E. *Can. J. Chem.* **1992**, *70*, 560−571.
(32) Dolg, M.; Stoll, H.; Preuss, H. *J. Chem. Phys.* **1989**, *90*, 1730−1734.
(33) Cao, X.; Dolg, M. *J. Chem. Phys.* **2001**, *115*, 7348−7355.
(34) Frisch, M. J.; Trucks, G. W.; Schlegel, H. B.; Scuseria, G. E.; Robb, M. A.; Cheeseman, J. R.; Scalmani, G.; Barone, V.; Mennucci, B.; Petersson, G. A.; et al. *Gaussian 09*, revision B.01; Gaussian, Inc.: Wallingford, CT, 2009.
(35) Becke, A. D. *Phys. Rev. A* **1988**, *38*, 3098−3100.
(36) Perdew, J. P. *Phys. Rev. B* **1986**, *33*, 8822−8824.
(37) Purvis, G. D., III; Bartlett, R. J. *J. Chem. Phys.* **1982**, *76*, 1910−1918.
(38) Raghavachari, K.; Trucks, G. W.; Pople, J. A.; Head-Gordon, M. *Chem. Phys. Lett.* **1989**, *157*, 479−483.
(39) Bartlett, R. J.; Musial, M. *Rev. Mod. Phys.* **2007**, *79*, 291−352.
(40) Kendall, R. A.; Dunning, T. H., Jr.; Harrison, R. J. *J. Chem. Phys.* **1992**, *96*, 6796−6806.
(41) Knowles, P. J.; Manby, F. R.; Schütz, M.; Celani, P.; Knizia, G.; Korona, T.; Lindh, R.; Mitrushenkov, A.; Rauhut, G.; Adler, T. B.; et al. *MOLPRO*, version 2010.1, a package of *ab initio* programs. See http://www.molpro.net.
(42) Watts, J. D.; Gauss, J.; Bartlett, R. J. *J. Chem. Phys.* **1993**, *98*, 8718−8733.
(43) Deegan, M. J. O.; Knowles, P. J.. *Chem. Phys. Lett.* **1994**, *227*, 321−326.
(44) Rittby, M.; Bartlett, R. J. *J. Phys. Chem.* **1988**, *92*, 3033−3036.
(45) Andrews, L. *J. Chem. Phys.* **1972**, *57*, 51−55.
(46) Andrews, L.; Raymond, J. I. *J. Chem. Phys.* **1971**, *55*, 3078−3086.
(47) Jacox, M. E. *J. Mol. Spectrosc.* **1980**, *84*, 74−88.
(48) Gabelnick, S. D.; Reedy, G. T.; Chasanov, M. G. *J. Chem. Phys.* **1974**, *60*, 1167−1171.
(49) DeKock, R. L.; Weltner, W., Jr. *J. Phys. Chem.* **1971**, *75*, 514−525.
(50) Kovácsa, A.; Konings, R. J. M. *J. Phys. Chem. Ref. Data* **2004**, *33*, 337 and references therein.
(51) Buchmarina, V. N.; Gerasimov, A. Yu.; Predtechenskii, Yu. B.; Shklyarik, V. G. *Opt. Spectrosc. (USSR)* **1992**, *72*, 38−40.
(52) Gong, Y.; Zhou, M. F.; Andrews, L. *Chem. Rev.* **2009**, *109*, 6765−6808.
(53) Milligan, D. E.; Jacox, M. E. *J. Chem. Phys.* **1968**, *48*, 2265−2271.
(54) Greenwood, N. N.; Earnshaw, A. *Chemistry of the Elements*; Pergamon Press: Oxford, U.K., 1994; Chapter 30, pp 1423−1449.
(55) Weinhold, F. In *Encyclopedia of Computational Chemistry*; P. v. R. Schleyer, Ed.; John Wiley & Sons: Chichester, U.K., 1998; Vol. 3, pp 1792−1811.
(56) Weinhold, F.; Landis, C. R., *Valency and Bonding: A Natural Bond Orbital Donor-Acceptor Perspective*; University Press: Cambridge, U.K., 2003.
(57) Reed, A. E.; Curtiss, L. A.; Weinhold, F. *Chem. Rev.* **1988**, *88*, 899−926.
(58) Reed, A. E.; Weinstock, R. B.; Weinhold, F. *J. Chem. Phys.* **1985**, *83*, 735−746.